Molecular Dynamics Simulations of the Melting Mechanisms of Perfect and Imperfect Crystals of Dimethylnitramine

Lianqing Zheng,[†] Betsy M. Rice,[‡] and Donald L. Thompson*[,†]

Department of Chemistry, University of Missouri-Columbia, Columbia, Missouri 65211, and U.S. Army Research Laboratory, AMSRD-ARL-WM-BD, Weapons and Materials Research Directorate, Aberdeen Proving Ground, Maryland 21005-5069

Received: October 12, 2006; In Final Form: January 17, 2007

The melting mechanisms of perfect and imperfect crystalline dimethylnitramine have been studied using molecular dynamics simulations. The imperfect crystal was created by removing ~10% of the molecules from the center of the simulation cell. The density, diffusion coefficient, translational and orientational order parameters, and void size were calculated as functions of temperature and simulation time. Upon melting, the volume of the imperfect crystal slowly decreases with time due to the shrinkage of the void then suddenly decreases to a minimum value due to collapse of the structure around the void with concomitant diffusion of molecules into the void. The simulation cell volume then increases as the liquid nucleus formed at the void expands. The melting of perfect crystals must occur by a different mechanism. As the temperature of the perfect crystal reaches the maximum superheating temperature, there is an increase in the thermal motions of the molecules that result in the formation of liquid centers (characterized by translational order parameter consistent with the liquid phase) at random locations. The liquid centers rapidly grow, resulting in a complete transition to the liquid phase. The increases in orientational and translational freedom occur simultaneously in the imperfect crystal, and in the perfect crystal, orientational freedom significantly precedes translational freedom.

1. Introduction

The microscopic details of how materials melt are of considerable practical value. Knowledge about the molecular-level behavior of processes can be used to formulate theories for predicting behavior obviating the need for measurements or expensive calculations. Assumptions about the molecular-level changes in solid-to-liquid transitions form the basis of the early theories of melting.[1,2] Molecular dynamics (MD) simulations can be used to probe the details of melting mechanisms and have been widely used for studies of Lennard-Jones and metallic solids, confirming the validity of the assumptions used to propose mechanisms for melting under various conditions. We are interested in exploring the effects of intramolecular degrees of freedom on melting; thus, we have been using MD simulations to study the melting of polyatomic molecular and ionic solids and nanoparticles and have reported a number of studies of a wide range of materials.[3] Our initial focus was on determining the accuracy of force fields and methods for using them in MD simulations to predict melting points. Direct heating of a perfect crystal results in superheating because of the free energy barrier to the formation of a solid−liquid interface. Fundamentally, melting is the breakup of the crystal lattice due to the development of points of instabilities. Heating a perfect infinite crystal leads to structural instabilities throughout it that form liquid nucleation sites. Thermodynamic melting starts at interfaces or defects in the solid.[4] The points of disruption in the crystal serve as nucleation centers for the formation of liquid droplets at the thermodynamic melting temperature, and melting in a perfect crystal occurs by homogeneous nucleation. Our interest in the present study are the details of homogeneous and heterogeneous nucleation melting mechanisms for a polyatomic molecular solid, namely, dimethylnitramine (DMNA), $(CH_3)_2$-NNO_2.

We recently reported studies of the superheated melting of nitromethane[5] and RDX (hexahydro-1,3,5-trinitro-1,3,5-*s*-triazine)[6] crystals that focused on changes in molecular conformations upon melting of perfect crystals. Although the molecular conformation of nitromethane undergoes little change upon melting due to its relative rigidity, the molecular conformation of the much larger cyclic nitramine RDX undergoes significant changes, mainly reorientation of the nitro groups that are attached to the triazine ring. The peaks in the distributions of most of the dihedral angles in the RDX molecules undergo pronounced broadening and/or shifting upon melting. Also, orientational disordering precedes translational disordering during melting. We have also examined the onset of disorder in surface-initiated melting of nitromethane.[7] The molecules first gain rotational freedom and then mobility when the melting begins at the crystal surface exposed to vacuum. The purpose of the present study is to investigate the molecular changes and the microscopic structural changes when melting begins at a void (Schottky defect)[8] and a perfect crystal of a molecule of flexibility intermediate between that of nitromethane and RDX. Simulating molecular solids with voids has been shown to be an effective *ad hoc* way of eliminating the superheating effect so that the thermodynamic melting point can be directly computed.[9−20] Void-induced melting corresponds to the practical laboratory conditions for measuring melting points; thus, it is important to understand the microscopic mechanism. Thus, it

* Corresponding author. E-mail: thompsondon@missouri.edu.
[†] Department of Chemistry.
[‡] U.S. Army Research Laboratory.

10.1021/jp0667184 CCC: $37.00
Published on Web 03/03/2007

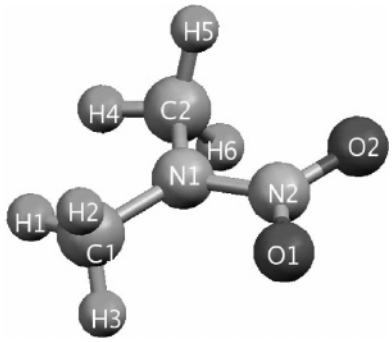

Figure 1. Molecular configuration of DMNA. The atom labels are used in the Results and Discussion.

is important that we understand the molecular and structural changes at a void as melting begins and spreads throughout a solid.

2. Computational Details

The structure of crystalline DMNA belongs to the monoclinic system, space group $P2_1/m$ ($Z = 2$, $a = 6.587$ Å, $b = 6.500$ Å, $c = 6.131$ Å, and $\beta = 123.13°$), at ambient conditions.[21] A DMNA molecule is shown in Figure 1 with atom labels that are used in the Results and Discussion. All the results were computed using the quantum-chemistry-based fully flexible force field developed by Smith et al.[22] This force field accurately reproduces the CNNO torsional barrier, NC_2 inversion barrier, and the thermodynamic melting point.[23] The values of the force field parameters are given in ref 22.

A supercell composed of $15 \times 15 \times 15$ unit cells (6750 molecules, 81 000 atoms) was used for the simulations of the perfect crystal. To compute the thermodynamic melting point it is necessary to introduce an interface in the crystal to overcome the superheating effect, which was done by creating a void by removal of molecules. The void may be of various kinds, ranging from planar arrays to randomly distributed molecular vacancies to spherical holes in the solid. In the present study, we created a spherical void of radius 13.0 Å centered at the center of mass of the supercell by removal of 80 molecules from a perfect crystal consisting of $7 \times 7 \times 8$ unit cells (784 molecules). This results in removal of ~10% of the molecules. This size void was chosen because it is sufficiently large to eliminate the superheating effect and yet will maintain the structural integrity of the crystal. When vacancies are introduced into a solid the computed melting point first decreases with increasing defect density but reaches a plateau region for a range of defect density. The thermodynamic melting point is determined by the average of the melting temperature in the plateau region. This plateau region for various kinds of solids has been found to occur when about 8% to 10% of the molecules are removed; see, e.g., ref 15.

The simulations were performed by using the DL_POLY program[24] for the isothermal−isobaric (*NPT*) ensemble.[25−27] The barostat allows the simulation cell edges to change isotropically while the cell angles remain constant. Three-dimensional periodic boundary conditions were applied. The relaxation times were the same for the thermostat and barostat, 1.0 and 0.5 ps, respectively, for the imperfect and perfect crystals. The integration time step for the trajectories was 1.0 fs. The cutoff distance was 10.0 Å for the van der Waals interactions. The electrostatic interactions were calculated using the smooth particle mesh Ewald algorithm.[28] The average value of the pressure in all simulations was constrained to 1 atm.

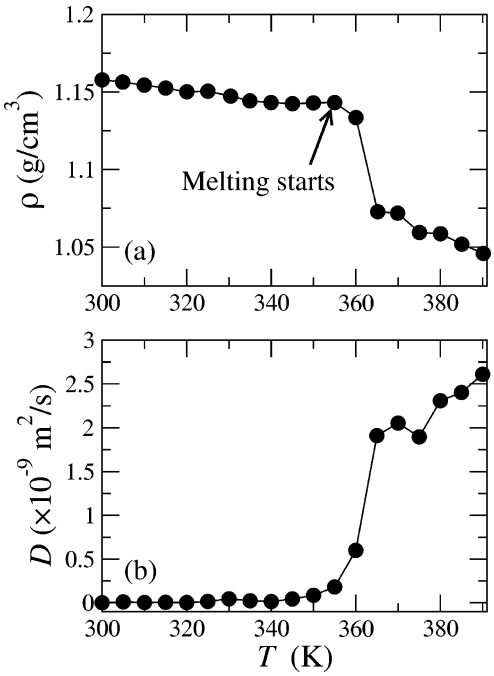

Figure 2. (a) Density ρ and (b) diffusion coefficient D as functions of temperature computed for the $7 \times 7 \times 8$ simulation cell with a void. The heating rate is 5.0×10^{10} K/s.

Incremental heating was used to raise the temperature from 300 K to a value above the melting points. For the simulations of the imperfect crystal, the system was equilibrated at 300 K, and then, the temperature was increased by 5 K increments at every 100 ps interval, which is equivalent to a heating rate of 5×10^{10} K/s. For the perfect crystal, the temperature was increased from 300 to 350 to 400 K after each 20 ps, after which it was increased by 10 K at every 20 ps interval, corresponding to a heating rate of 5.0×10^{11} K/s. We found that 100 or 20 ps was not long enough for the simulation cell to reach equilibrium at the temperatures where the melting started; thus, we extended the simulation time up to 600 and 200 ps at those temperatures (see below) for the imperfect and perfect crystals, respectively.

Order parameters are good measures of the extent of melting. Following the definitions in our previous papers,[5,6] we define the translational (ψ^T) and orientational (ψ^O) order parameters as

$$\psi^{\mathrm{T}} = \frac{1}{N_{\mathrm{m}}} \sum_{i=1}^{N_{\mathrm{m}}} \left| \cos\left(2\pi \frac{\mathbf{r}_i^{\mathrm{ref}} \cdot \mathbf{r}_i}{(\mathbf{r}_i^{\mathrm{ref}})^2} \right) \right|^2 \qquad (1)$$

and

$$\psi^{\mathrm{O}} = \frac{1}{N_{\mathrm{m}}} \sum_{i=1}^{N_{\mathrm{m}}} (\mathbf{n}_{\mathrm{NN},i} \cdot \mathbf{n}_{\mathrm{NN},i}^{\mathrm{ref}})^2 \qquad (2)$$

Here, N_m is the number of molecules in the supercell, and the vectors $\mathbf{r}_i$ and $\mathbf{n}_{NN,i}$ are, respectively, the coordinates of the center of mass and normal vector of the N−N bond of the i-th molecule. The superscript "ref" denotes the values expected when the MD simulation cell undergoes only linear thermal expansion.

3. Results and Discussion

3.1. Melting of Crystals with a Void. Figure 2 shows the density ρ, frame a, and diffusion coefficient D, frame b, of the

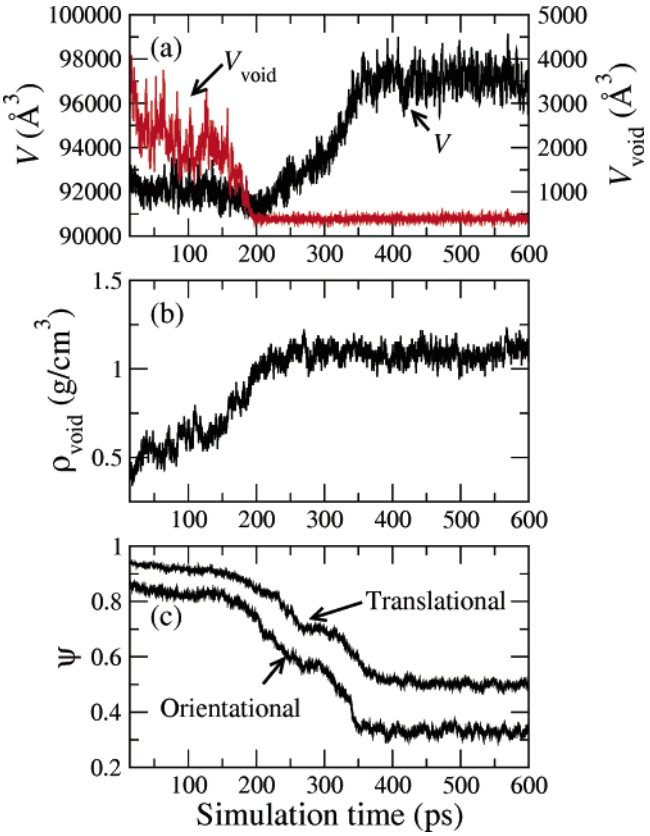

Figure 3. (a) Simulation cell volume V (black curve) and void volume V_{void} (red curve), (b) density of the material in the original void ρ_{void}, and (c) translational and orientational order parameters as functions of simulation time at 355 K.

simulation cell as functions of temperature for a heating rate of 5 K/100 ps. When the temperature is increased from 355 to 360 K, both ρ and D undergo abrupt changes. However, the melting actually starts at 355 K, and the initial simulation time of 100 ps is not long enough for the melting process to finish. We then extended the simulation time to 600 ps. The melting temperature T_{mp} is 355 K, which is higher than both the thermodynamic melting point (330 K) obtained in a previous study of void-induced melting[23] and the experimental value of 331 K.[21] The difference in the computed melting point values is due to the difference in the heating rates. The heating rate in the present study is much larger than in the previous study.[23] The correct thermodynamic melting point may require a lower heating rate than that used here. We have chosen to use a heating rate that allows us to carry out an investigation of the mechanism given a reasonable expenditure of computer time. The mechanism for true thermodynamic melting could differ some from what we report here; however, we believe that it would not be qualitatively different.

The volume of the simulation cell V and that of the void V_{void} as functions of time are shown in Figure 3a; the density of the material within the original void (ρ_{void}) and the translational and orientational order parameters as functions of time during the portion of the simulation for which the temperature is set to 355 K are shown in Figure 3b, c, respectively. The volume of the void, which we assume to be spherical during the simulation, is calculated using an effective void radius, defined as follows. The simulation cell is divided into 20 × 20 × 20 grid points, and for each grid point, we find the nearest molecule on the basis of the distances between molecular centers of mass and the grid point. The center of the void is located at the grid point that has the longest distance to the nearest molecule; this

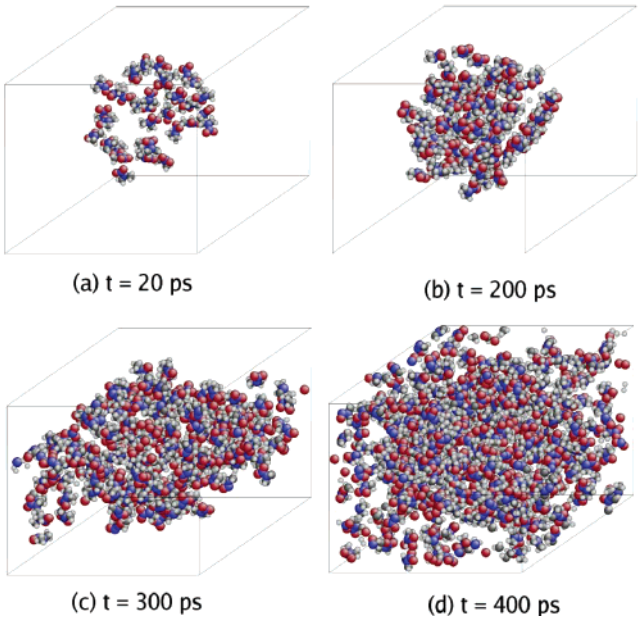

Figure 4. Snapshots of only the *liquid molecules* at different stages of the melting the 7 × 7 × 8 simulation cell with void. The temperature is 355 K, and the time is consistent with that in Figure 3. The *liquid molecules* are defined as those with local translational order parameters (see eq 1) less than or equal to 0.5, which is the average value of the translational order parameter for the liquid phase.

distance is taken to be the radius of the void, which is used to determine the volume of the void. A similar approach has been used in ref 29. To calculate ρ_{void}, we first find the center of the void in the initial simulation cell, then assume that a molecule is in the original void if its center of mass is within a distance from the center of the void less than or equal to the original void radius (13.0 Å).

As shown by the results in Figure 3a, the volumes of both the simulation cell and the void slowly decrease with time up to about 150 ps. Concurrently, the density within the region defined by the original void increases as molecules diffuse into it; see Figure 3b. There is a sharp drop in the volume of the simulation cell at ~150 ps, and it reaches a minimum value at 200 ps. After 200 ps, the volume of the simulation cell increases rapidly to reach the value for liquid. The volume of the void, on the other hand, sharply decreases between 150 to 200 ps, after which it oscillates about an average value of 400 Å^3. The average final value of the void radius is about 4.5 Å, close to half of the first minimum distance in the center of the mass radial distribution function (not shown) of the DMNA liquid phase. The translational and orientational order parameters as functions of time are shown in Figure 3c; their values are initially about 0.94 and 0.86, respectively. They slowly decrease until the void starts to collapse at about 200 ps, after which (over the time interval 200−350 ps) they decrease much faster than in the earlier portion of the trajectory. The final values are about 0.5 and 0.35 for the translational and orientational order parameters, respectively. The positional and orientational disordering occurs simultaneously.

To investigate the microscopic details of the melting mechanisms, we define *liquid molecules* as those with local translational order parameters less than or equal to 0.5, which is the average value of the translational order parameter for the liquid phase. Snapshots of only the *liquid molecules* at different times in the simulation for 355 K are shown in Figure 4.[30] The results shown in Figure 4 were obtained from the same simulation as those shown in Figure 3. At 20 ps (see Figure 4a), the *liquid*

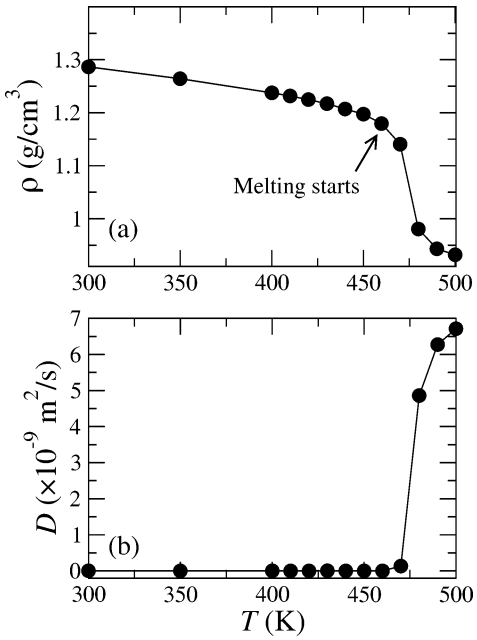

Figure 5. (a) Density ρ and (b) diffusion coefficient D as functions of temperature for the 15 × 15 × 15 perfect crystal. The heating rate is 5.0 × 10^{11} K/s.

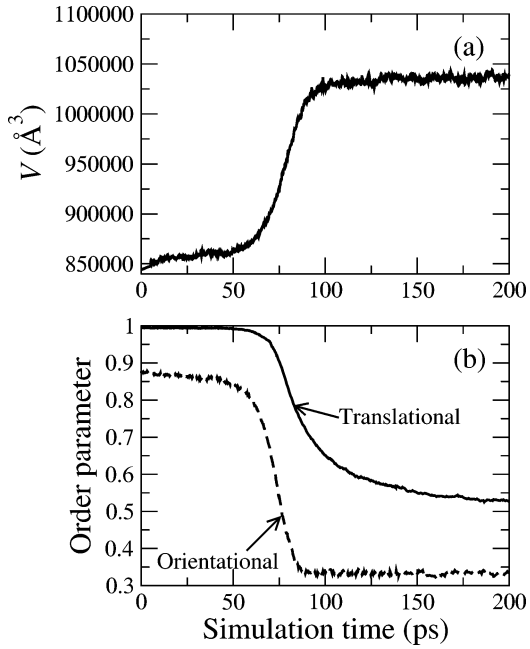

Figure 6. (a) Simulation cell volume V and (b) translational and orientational order parameters for the 15 × 15 × 15 simulation cell (perfect crystal) as functions of the simulation time at 460 K.

molecules are only on the surface area of the void. The number of the *liquid molecules* continues to increase with time and diffuse into the void, as illustrated in Figure 4b, which is the snapshot at 200 ps. The liquid nucleus formed at the void space rapidly propagates throughout the solid, as illustrated in Figure 4c, d.

3.2. Melting of the Perfect Crystal. Figure 5 shows the density and diffusion coefficient as functions of temperature for the simulations of the perfect crystal. The value at each temperature shown in Figure 5 was obtained with a heating rate of 10 K/20 ps. There is an abrupt change between 460 and 470 K. The melting actually starts when the temperature is increased from 450 to 460 K, as manifested by consistently increasing simulation cell volume with time. These results show that 20 ps is not long enough to allow for complete melting; therefore, we extended the simulation time from 20 to 200 ps at 460 K. The maximum superheating temperature, 460 K, is also higher than the value, 420 K, obtained by Bedrov et al.[23] for this force field. The difference is likely due to the fact that the heating rates used in the two studies are not exactly the same.

The simulation cell volume and translational and orientational order parameters at 460 K as functions of the simulation time are shown in Figure 6. Unlike the behavior observed in the melting of a crystal with a void, the translational order parameter in the perfect crystal changes much more slowly than the orientational order parameter and the volume. The orientational order parameter and the volume reach equilibrium values almost at the same time (~80 ps), and it takes at least 200 ps for the translational order parameter to reach an equilibrium value. This shows that the orientational disordering of a perfect crystal upon melting significantly precedes the translational one, which is consistent with what we found in simulations of the perfect RDX crystal.[6]

The nucleation process, due to random fluctuations in the solid that initiates melting of the perfect crystal, is illustrated by the snapshots shown in Figure 7, in which only the *liquid molecules* are depicted. The results in Figure 7 are for a simulation at 460 K. We see a few *liquid molecules* at 40 ps (see Figure 7a) in the simulation cell; a few more *liquid*

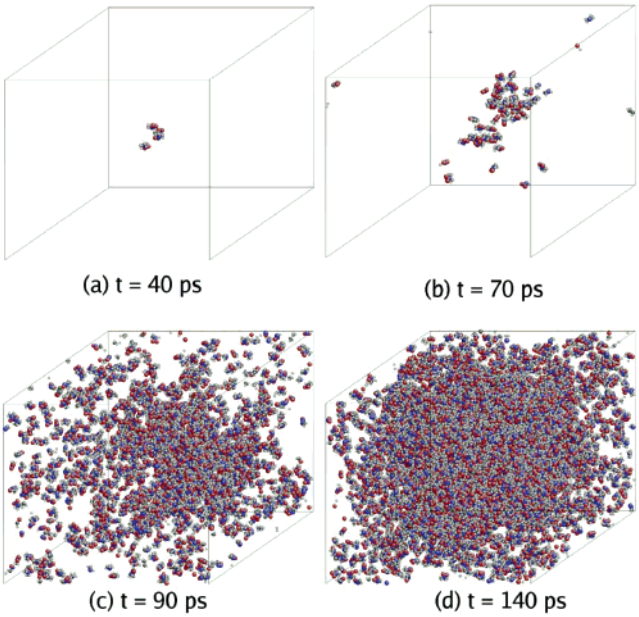

Figure 7. Snapshots of only the *liquid molecules* at different stages of the melting of the 15 × 15 × 15 perfect crystal. Other results of the simulation are shown in Figure 6. The *liquid molecules* are defined as those with local translational order parameters (see eq 1) less than or equal to 0.5, which is the average value of the translational order parameter for the liquid phase.

molecules are present at random locations at 70 ps, and a few liquid nuclei are clearly seen (see Figure 7b). The rapid growth of the liquid nucleus (or nuclei) occurs between 70 and 90 ps as we see a tremendous increase in the number of *liquid molecules* at 90 ps (see Figure 7c), which continues until the melting is complete (see Figure 7d).

4. Summary and Conclusions

We have studied the details of homogeneous and heterogeneous nucleation melting mechanisms for crystalline

dimethylnitramine. The mechanisms were investigated by using MD simulations with incremental heating. Imperfect crystalline DMNA was represented by a simulation cell with a void located at its center created by removing ~10% of the molecules from a perfect crystal. Changes in the density, diffusion coefficient, orientational and translational order parameters, and void size (in the case of the imperfect crystal) with the temperature and simulation time are the key quantities that were monitored.

In the melting of the imperfect crystal, the first stage is the shrinkage of the void with a corresponding decrease in the volume of the crystal. By defining *liquid molecules* as having a local translational order parameter less than or equal to the average of the value for the liquid phase (0.5), we can show that liquid nucleation originates on the free surface of the void. There is a sudden drop in the void size to a minimum value as the molecules initially on the free surface of the void diffuse into the vacant space. Subsequently, the simulation cell volume increases as the liquid nucleus formed at the void rapidly propagates out into the solid portion of the crystal. When the temperature reaches the maximum superheating temperature of the perfect crystal, the increased thermal motions of the molecules result in the formation of *liquid molecules* at random locations in the solid that aggregate into larger clusters, which rapidly grow and propagate throughout the solid, resulting in the full transition to the liquid phase. The progress of orientational and positional disorder occurs simultaneously in the melting of the imperfect crystal, and orientational disordering significantly precedes translational freedom in the case of the perfect crystal.

Acknowledgment. This work was supported by a MURI grant managed by the Army Research Office.

References and Notes

(1) (a) Born, M. *J. Chem. Phys.* **1939**, *7*, 591. (b) *Proc. Cambridge Philos. Soc.* **1940**, *36*, 160.

(2) Lindemann, F. A. *Phys. Z.* **1910**, *11*, 609.

(3) For a review of these studies, see Alavi, S.; Thompson, D. L. *Mol. Simul.* **2006**, *32*, 999.

(4) See, e.g., (a) Daeges, J.; Gleiter, H.; Perepezko, J. H. *Phys. Lett. A* **1986**, *119*, 79. (b) Cahn, R. W. *Nature (London)* **1986**, *323*, 668. (c) Maddox, J. *Nature (London)* **1987**, *330*, 599.

(5) Zheng, L.; Luo, S. N.; Thompson, D. L. *J. Chem. Phys.* **2006**, *124*, 154504.

(6) Zheng, L.; Thompson, D. L. *J. Chem. Phys.* **2006**, *125*, 084505.

(7) Siavosh-Haghighi, A.; Thompson, D. L. *J. Chem. Phys.* **2006**, *125*, 184711.

(8) Kittel, C. *Introduction to Solid State Physics*, 5th ed.; Wiley: New York, 1976; p 538.

(9) Phillpot, S. R.; Lutsko, J. F.; Wolf, D.; Yip, S. *Phys. Rev. B* **1989**, *40*, 2831.

(10) Lutsko, J. F.; Wolf, D.; Phillpot, S. R.; Yip, S. *Phys. Rev. B* **1989**, *40*, 2841.

(11) Solca, J.; Dyson, A. J.; Steinebrunner, B.; Kirchner, B.; Huber, H. *Chem. Phys.* **1997**, *224*, 253.

(12) Solca, J.; Dyson, A. J.; Steinebrunner, B.; Kirchner, B.; Huber, H. *J. Chem. Phys.* **1998**, *108*, 410.

(13) Agrawal, P. M.; Rice, B. M.; Thompson, D. L. *J. Chem. Phys.* **2003**, *118*, 9680.

(14) Velardez, G. F.; Alavi, S.; Thompson, D. L. *J. Chem. Phys.* **2003**, *119*, 6698.

(15) Agrawal, P. M.; Rice, B. M.; Thompson, D. L. *J. Chem. Phys.* **2003**, *119*, 9617.

(16) Velardez, G. F.; Alavi, S.; Thompson, D. L. *J. Chem. Phys.* **2004**, *120*, 9151.

(17) Alavi, S.; Thompson, D. L. *J. Chem. Phys.* **2005**, *122*, 154704.

(18) Alavi, S.; Thompson, D. L. *J. Phys. Chem. B* **2005**, *109*, 18127.

(19) Agrawal, P. M.; Rice, B. M.; Zheng, L.; Velardez, G. F.; Thompson, D. L. *J. Phys. Chem. B* **2006**, *110*, 5721.

(20) Zheng, L.; Thompson, D. L. *J. Phys. Chem. B* **2006**, *110*, 16082. Some of the results reported in this paper are in error; see ref 23.

(21) Filhol, A.; Bravic, G.; Rey-Lafon, M.; Thomas, M. *Acta Crystallogr.* **1980**, *B36*, 575.

(22) Smith, G. D.; Bharadwaj, R. K.; Bedrov, D.; Ayyagari, C. *J. Phys. Chem. B* **1999**, *103*, 705.

(23) Bedrov, D.; Borodin, O.; Hanson, B.; Smith, G. G. *J. Phys. Chem. B* **2007**, *111*, 1900.

(24) Forester, T. R.; Smith, W. *DL_POLY, CCLRC*; Daresbury Laboratory: Cheshire, U.K., 1995.

(25) Nosé, S. *J. Chem. Phys.* **1984**, *81*, 511.

(26) Hoover, W. G. *Phys. Rev. A* **1985**, *31*, 1695.

(27) Melchionna, S.; Ciccotti, G.; Holian, B. L. *Mol. Phys.* **1993**, *78*, 533.

(28) Essmann, U.; Perera, L.; Berkowitz, M. L.; Darden, T.; Lee, H.; Pedersen, L. G. *J. Chem. Phys.* **1995**, *103*, 8577.

(29) Muralidharan, K.; Simmons, J. H.; Deymier, P. A.; Runge, K. J. *Non-Cryst. Solids* **2005**, *351*, 1532.

(30) The software AtomEye was used to generate Figures 4 and 7; see Li, J. *Modell. Simul. Mater. Sci. Eng.* **2003**, *11*, 173.